LETTER

doi:10.1038/nature20125

Cultural innovation and megafauna interaction in the early settlement of arid Australia

Giles Hamm[1], Peter Mitchell[2], Lee J. Arnold[3], Gavin J. Prideaux[4], Daniele Questiaux[5], Nigel A. Spooner[5,6], Vladimir A. Levchenko[7], Elizabeth C. Foley[1], Trevor H. Worthy[4], Birgitta Stephenson[8,9], Vincent Coulthard[10], Clifford Coulthard[10], Sophia Wilton[10] & Duncan Johnston[10]

Elucidating the material culture of early people in arid Australia and the nature of their environmental interactions is essential for understanding the adaptability of populations and the potential causes of megafaunal extinctions 50–40 thousand years ago (ka). Humans colonized the continent by 50 ka[1,2], but an apparent lack of cultural innovations compared to people in Europe and Africa[3,4] has been deemed a barrier to early settlement in the extensive arid zone[2,3]. Here we present evidence from Warratyi rock shelter in the southern interior that shows that humans occupied arid Australia by around 49 ka, 10 thousand years (kyr) earlier than previously reported[2]. The site preserves the only reliably dated, stratified evidence of extinct Australian megafauna[5,6], including the giant marsupial *Diprotodon optatum*, alongside artefacts more than 46 kyr old. We also report on the earliest-known use of ochre in Australia and Southeast Asia (at or before 49–46 ka), gypsum pigment (40–33 ka), bone tools (40–38 ka), hafted tools (38–35 ka), and backed artefacts (30–24 ka), each up to 10 kyr older than any other known occurrence[7,8]. Thus, our evidence shows that people not only settled in the arid interior within a few millennia of entering the continent[9], but also developed key technologies much earlier than previously recorded for Australia and Southeast Asia[8].

Ten archaeological sites, between 41 and 28 kyr in age, have previously been recorded from arid Australia[10] (Fig. 1). Many lack well-stratified deposits and very few span durations of more than 20 kyr. The scarcity of late Pleistocene sites, especially in the southern arid interior, continues to prevent reliable interpretations of the nature, timing and implications of human colonization across the continent. Warratyi rock shelter provides important new evidence for the early occupation of arid Australia. The site is an elevated rock shelter located in the Adnyamathanha country within the present arid zone at the northern end of the Flinders Ranges, in the southern Lake Eyre Basin, South Australia (Fig. 1). The shelter contains a stratified, 1-m-deep, intact archaeological deposit composed of four stratigraphic units (SU1–SU4; Fig. 2, Extended Data Figs 1–3 and Supplementary Information: stratigraphy).

Single-grain optical dating (optically stimulated luminescence (OSL) and thermally-transferred OSL (TT-OSL)) of quartz grains and radiocarbon (^{14}C) dating of hearth charcoal and avian eggshells were used to establish the occupation chronology (Fig. 2). The oldest layer (SU4) yielded calibrated ^{14}C ages of deposition of >46.0 and >44.7 ka (mean calibrated ages ± 68% probability ranges = 48.2 ± 1.2 and 47.3 ± 1.5 kyr) based on an eggshell of a large extinct megapode bird[6] (see Supplementary Information: megafauna), and a ^{14}C-calibrated age of 49.2–46.3 ka, based on an emu eggshell (Fig. 2). All are within 2 standard errors of two associated optical ages of 43.8 ± 3.4 ka and 42.8 ± 2.4 ka (Extended Data Fig. 6). The age of the overlying SU3 is constrained by five ^{14}C ages with a combined span of 41.0–32.7 ka and optical ages of 40.5 ± 2.2 and 30.3 ± 1.6 ka. Deposition of SU2 is constrained to 29.8–24.4 ka from Bayesian modelling of one optical age and four ^{14}C ages, while three optical ages reveal that SU1B accumulated 11.8–9.9 ka, with post-depositional bioturbation resulting in younger eggshells being incorporated into this unit (see Extended Data Fig. 7 and Supplementary Information: chronology). These ages isolate Warratyi rock shelter as the only site outside of tropical northern Australia with a rich, stratified record of repeated human activity spanning 50–10 ka.

Stone artefacts were found throughout the deposit (Fig. 2) with concentrations at depths of 5–20 cm (corresponding to SU1–upper part SU2) and 60–80 cm (SU3). The lithic assemblage is mostly composed of whole flakes, broken flakes and waste material. Stone artefacts were made from a range of raw materials, reflecting a change in use of preferred rock-type over time. Tools in the lowermost units were predominantly made of quartz. In the upper part of SU2 and in SU1, chert and silcrete become major components. This pattern was also reflected by changes in tool types; SU1 and SU2 contained predominately backed and small hafted tools, whereas SU3 and SU4 contained whole and retouched flakes (Extended Data Fig. 5). The chronology revealed by Bayesian modelling of all stratigraphically reliable ages available for Warratyi greatly extends the antiquity of backed and hafted tools in Australia. The oldest backed artefacts, three geometric microliths found in SU2 at a depth of 25 cm (Fig. 2), have a Bayesian modelled age of deposition of 30–24 ka. The previous oldest confirmed deposition ages are 4 ka in the arid zone[10] and 8.5 ka on the east coast[7]. A possible occurrence of 15 ka has been reported from rock-shelter site GRE8 in the Carpentarian Gorges, northern Queensland (Fig. 1), but interpretation of its stratigraphic context has been questioned[10,11]. Residue analysis identified resin within SU3 (70–75cm depth), which shows that some flakes had been hafted (see Extended Data Fig. 8A and Supplementary Information: residues). Our modelling produced a deposition age of 40–33 ka for this unit, showing that this is by far the earliest-known evidence of hafting technology in Australia and Southeast Asia. The previous oldest ages were early Holocene (10–9 ka)[12,13].

White spheroids (diameter 2–30 mm) were found at depths of 20–75 cm in SU2–SU3 (40–24 ka). X-ray diffraction analysis identified the material in the spheres as gypsum (see Extended Data Fig. 8B and Supplementary Information: gypsum), the closest known source of which is 12–15 km to the north. We interpret this gypsiferous material as having been brought to the rock shelter for making white pigment. X-ray diffraction was also used to confirm the presence of red ochre,

[1]Department of Archaeology and History, La Trobe University, Melbourne, Victoria 3083, Australia. [2]Geomorphic Consultant Gladesville, Sydney 2111, New South Wales, Australia. [3]School of Physical Sciences, the Environment Institute and the Institute for Photonics and Advanced Sensing, University of Adelaide, Adelaide, South Australia 5005, Australia. [4]School of Biological Sciences, Flinders University, Adelaide, South Australia 5001, Australia. [5]Institute for Photonics and Advanced Sensing, School of Physical Sciences, University of Adelaide, Adelaide, South Australia 5005, Australia. [6]Defence Science and Technology Group, Edinburgh, Adelaide, South Australia 5111, Australia. [7]Australian Nuclear Science and Technology Organisation, Lucas Heights, Sydney, New South Wales 2234, Australia. [8]In the Groove Analysis Pty Ltd, Indooroopilly, Brisbane, Queensland 4068, Australia. [9]School of Social Sciences, University of Queensland, St Lucia, Brisbane, Queensland 4072, Australia. [10]Adnyamathanha Traditional Lands Association, Port Augusta, South Australia 5700, Australia.

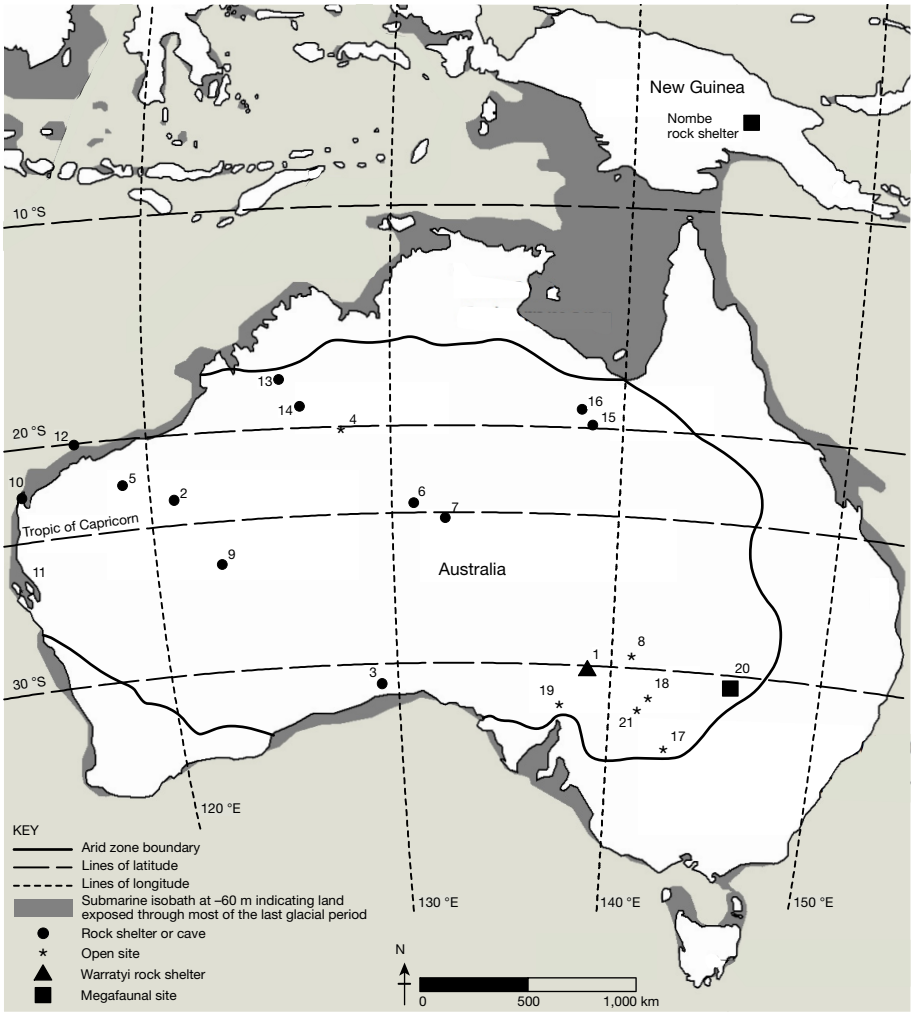

Figure 1 | Site distribution map showing archaeological and megafaunal sites. Site distribution map with sea level at the −60 m contour showing the geographical location of known Australian arid zone archaeological and megafaunal sites with age ranges discussed in the text. Arid interior sites 1−9, arid west coast sites 10 and 11, northern desert margins sites 13−16, southeast desert margins sites 17−21. 1, Warratyi rock shelter, 49–45 kyr in age; 2, Djadjiling and Newman P2055, 41–30 kyr in age; 3, Allens Cave, 40 kyr in age; 4, Lake Gregory, >37 kyr in age; 5, Juukan 1, 37 kyr in age; 6, Puritjarra, 35 kyr in age; 7, Kulpi Mara, 34–29 kyr in age; 8, Lake Yantara, 31 kyr in age; 9, Serpents Glen, 28 kyr in age; 10, Northwest Cape sites (Jansz, Mandu Mandu, C99 and Pilgonaman), 40–24 kyr in age; 11, Silver Dollar, 35–22 kyr in age; 12, Noala, 31 kyr in age; 13, Carpenters Gap 1, 48–44 kyr in age; 14, Riwi, 45–34 kyr in age; 15, GRE8, 39–31 kyr in age; 16, Colless Creek, 30 kyr in age; 17, Lake Mungo and Willandra Lakes sites, 50–40 kyr in age; 18, Lake Menindee, 45 kyr in age; 19, Dempseys Lake, 44 kyr in age; 20, Cuddie Springs, 39–35 kyr in age; 21, Lake Tandou, 41–31 kyr in age. Archaeological sites are either open sites or rock shelters mapped within the modern Australian arid zone boundary and the Tropic of Capricorn. Megafaunal sites, black squares; rock shelters, circles; open sites, asterisks. The map also shows the general location of Warratyi rock shelter (triangle symbol) (from ref. 10).

with the lowest sample found in SU4 in association with artefacts and bone material (≥49–46 kyr in age; Fig. 2 and Supplementary Information: red ochre). Residue analysis confirmed the presence of worked red ochre on a silcrete stone tool in SU4 at a depth of 90 cm (see Supplementary Information: residues). The earliest previous evidence for the use of ochre in Australia and Southeast Asia is 42.8 ka at Carpenters Gap rock shelter[14,15]. No archaeological evidence for the pre-modern use of gypsum has hitherto been reported from Australia.

At least 16 species of mammal and 1 reptile were identified from a representative sub-sample of the Warratyi bone assemblage (see Supplementary Information: fauna). More than 2,000 fragments were assessed, revealing a predominance of medium-sized macropodids. Bones lacked evidence of animal gnawing or breakage patterns caused by predators or scavengers, supporting the interpretation that they accumulated as a result of human activity. A sharpened bone point, ground from the cylindrical portion of the proximal end of a macropodid fibula (similar to a yellow-footed rock-wallaby, *Petrogale xanthopus*), was recovered from a depth of 65–70 cm (SU3, Figs 2, 3). Similar single-point tools have been interpreted elsewhere as having been used for fine needle or awl work on animal skins[16]. Bone tools have been considered a late Pleistocene innovation for humans in Australia and East Timor, but only appeared in the last 11 kyr in the rest of Southeast Asia[17,18]. The stratigraphic position of this tool indicates an age of >38 kyr, which is substantially older than the next youngest examples found at Wareen Cave (29 kyr in age) in Tasmania[19] and Devils Lair (26 kyr in age) in south-western Australia[20,21].

A partial right juvenile radius of a rhino-sized marsupial herbivore *D. optatum* and possibly burnt and unburnt fragments of an egg-shell of a large, ground-nesting megapode bird[6] (shell type formerly identified as *Genyornis newtoni*; see refs 22–25) were recovered from a depth of 85–90 cm (Extended Data Figs 9, 10). Direct ^{14}C dating of the shell and optical dating of host sediments indicated a deposition age of ≥49–46 ka (SU4, Fig. 2). The age of these fossils, together with the absence of carnivore tooth marks and the position of the shelter on a steep escarpment unsuitable for climbing by individuals of *D. optatum* (see Supplementary Information: stratigraphy), indicate co-occurrence of these taxa with humans who were probably involved in the accumulation of their remains.

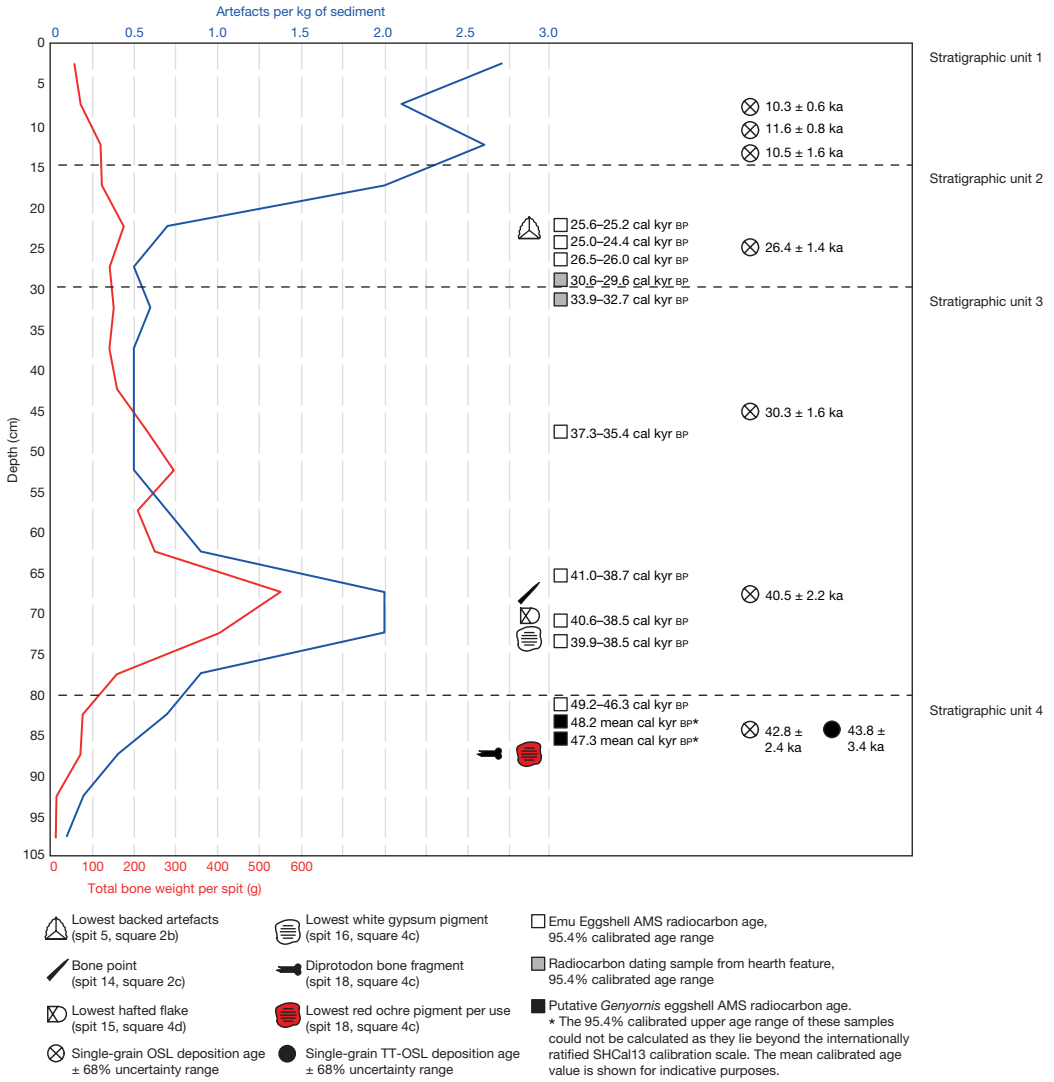

Figure 2 | Main chrono–stratigraphic and archaeological features found in Warratyi rock shelter. A graphical depiction of the distribution of artefacts and bone against depth below the surface, and the inferred stratigraphic units (1–4) in Warratyi rock shelter showing overall site chronology and important artifacts found at the site. The depth of dated samples and their ages are indicated. The density of artefacts (number per kilogram of sediment) is shown in blue and weight (g) of bone in red. White squares, emu eggshell ages; black squares, putative *Genyornis* oological material eggshell ages; white and black circles, single-grain OSL and TT-OSL ages, respectively. AMS, accelerator mass spectrometry.

Warratyi rock shelter is the oldest Australian arid-zone occupation site and one of the earliest on the continent. The presence of people in the southern interior of the continent ≥49–46 ka (Fig. 1) suggests that, following their arrival in Australia, people dispersed more rapidly across the continent than previously thought. The location of Warratyi could imply a more direct north–south route for pioneering human settlers rather than an exclusive coastal route. The evidence supports the model that Aboriginal people had settled in the Australian arid zone well before the extreme arid conditions of the last glacial maximum and the associated expansion of major environmental barriers such as sandy deserts[9].

Human occupation was repeated but ephemeral in nature, indicating that Aboriginal people may have used Warratyi both as a refuge at a time when the surrounding lowlands and open plains were too arid to exploit and as a temporary campsite when environmental conditions became more stable regionally[10].

The development of worked-bone technology by at least 40–38 ka, hafted tools by at least 35 ka and backed artefacts by at least 24 ka shows that people living at Warratyi were early innovators of modern technological adaptations found in late Pleistocene Australia and Southeast Asia. This refutes previously held views concerning the timing of cultural and technological innovation for late Pleistocene Australia[8].

Warratyi also provides stratified archaeological data and a chronology that directly link humans with megafauna in Australia. The late Pleistocene is marked by the extinction of large vertebrates from the continents[22–24]. Although at least 22 species, which later went extinct, overlapped temporally with humans in Australia and New Guinea[22], only two sites, Cuddie Springs in eastern Australia and Nombe rock shelter in New Guinea (Fig. 1), have been reported to contain cultural and megafaunal material within the same stratigraphic layers[22,24]. However, the evidence of direct association between megafauna and humans at these sites has been challenged based on site formation, climatic, stratigraphic and chronological grounds[26–28].

The discovery of megafaunal bone and directly dated eggshell in a well-stratified and reliably dated archaeological context at Warratyi not only shows that these taxa were contemporary with humans but also provides the only direct evidence that people interacted with some megafauna in Australia. The location of Warratyi in northern South Australia is also important for evaluating the causes of continent-wide megafaunal extinction, because it confirms the temporal overlap of humans and extinct species 50–40 ka across a much broader geographic area of Australia than previously thought. Until now, direct evidence for the co-existence of humans and megafauna had been lacking for the arid interior, a major region of the continent.

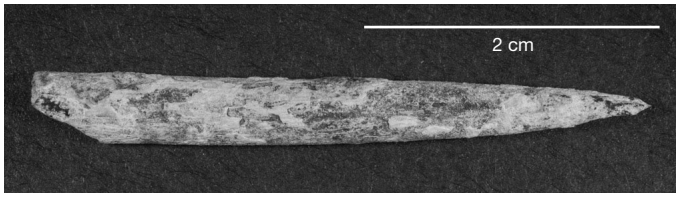

Figure 3 | Earliest bone point. A sharpened bone point, likely to be ground from the cylindrical portion of the proximal end of a macropod fibula similar in size to that of *Petrogale xanthopus*, the yellow-footed rock-wallaby. This specimen was found in SU3, dated to 40–38 ka and is currently the oldest bone point in Australia.

Archaeological sites with evidence of modern human colonisation, unique cultural innovation and interaction with now-extinct megafauna are rare in southern Asia and Australia. Sites preserving 50-kyr records of human occupation are rarer still. In addition to these landmark discoveries, Warratyi rock shelter reveals evidence for the development of modern human behaviour in Australia and Asia. Important technological innovations and early symbolic behaviour[9,29] reveal that a dynamic, adaptive Aboriginal culture existed in arid Australia within only a few millennia of settlement on the continent.

Online Content Methods, along with any additional Extended Data display items and Source Data, are available in the online version of the paper; references unique to these sections appear only in the online paper.

Received 26 May; accepted 27 September 2016.
Published online 2 November 2016.

1. Veth, P. & O'Connor, S. in *Cambridge History of Australia, Volume 1 Colonial Australia* (eds Bashford, A. & Macintyre, S.) 1–34 (Cambridge Univ. Press, 2013).
2. Allen, J. & O'Connell, J. Both half right: updating the evidence for dating first human arrivals in Sahul. *Aust. Archaeol.* **79,** 86–108 (2014).
3. Mellars, P. Going east: new genetic and archaeological perspectives on the modern human colonization of Eurasia. *Science* **313,** 796–800 (2006).
4. Boivin, N., Fuller, D. Q., Dennel, R., Allaby, R. & Petraglia, M. D. Human dispersal across diverse environments of Asia during the Upper Pleistocene. *Quat. Int.* **300,** 32–47 (2013).
5. Roberts, R. G. *et al.* New ages for the last Australian megafauna: continent-wide extinction about 46,000 years ago. *Science* **292,** 1888–1892 (2001).
6. Grellet-Tinner, G., Spooner, N. A. & Worthy, T. H. Is the '*Genyornis*' egg of mihirung or another extinct bird from the Australian dreamtime? *Quat. Sci. Rev.* **133,** 147–164 (2016).
7. Attenbrow, V., Robertson, G. & Hiscock, P. The changing abundance of backed artefacts in south-eastern Australia: a response to Holocene climate change? *J. Archaeol. Sci.* **36,** 2765–2770 (2009).
8. Habgood, P. J. & Franklin, N. R. The revolution that didn't arrive: a review of Pleistocene Sahul. *J. Hum. Evol.* **55,** 187–222 (2008).
9. Hiscock, P. & Wallis, L. in *Desert Peoples: Archaeological Perspectives* (eds Veth, P., Smith, M. & Hiscock, P.) 34–57 (Blackwell Publishers, 2005).
10. Smith, M. *The Archaeology of Australia's Deserts* (Cambridge Univ. Press, 2013) 185–187.
11. Slack, M. J., Fullagar, R. L. K., Field, J. H. & Border, A. New Pleistocene ages for backed artefact technology in Australia. *Archaeol. in Oceania* **39,** 131–137 (2004).
12. Mulvaney, D. J. & Kamminga, J. *The Prehistory of Australia* (Allen & Unwin Pty Ltd, 1999).
13. Barton, H. M., Piper, P. J., Rabett, R. & Reeds, I. Composite hunting technologies from the terminal Pleistocene and early Holocene, Niah Cave Borneo. *J. Archaeol. Sci.* **36,** 1708–1714 (2009).
14. O'Connor, S. & Frankhauser, B. in *Histories of Old Ages: Essays in Honour of Rhys Jones* (eds Anderson, A., Lilley, I. & O'Connor, S.) 287–300 (Pandanus Books, Research School of Pacific and Asian Studies, Australian National Univ., 2001).
15. Aubert, M. *et al.* Pleistocene cave art from Sulawesi, Indonesia. *Nature* **514,** 223–227 (2014).
16. Webb, C. & Allen, J. A functional analysis of Pleistocene bone tools from two sites in southwest Tasmania. *Archaeol. in Oceania* **25,** 75–78 (1990).
17. O'Connor, S., Robertson, G. & Aplin, K. P. Are osseous artefacts a window to perishable material culture? Implications of an unusually complex bone tool from the Late Pleistocene of East Timor. *J. Hum. Evol.* **67,** 108–119 (2014).
18. Rabett, J. R. The early exploitation of South-east Asian mangroves: bone technology from caves and open sites. *Asian Perspect.* **44,** 154–179 (2005).
19. Cosgrove, R. Forty two degrees south: the archaeology of Late Pleistocene Tasmania. *J. World Prehist.* **13,** 357–402 (1999).
20. Dortch, C. E. *Devil's Lair, A Study in Prehistory* (Western Australian Museum, 1984).
21. Dortch, C. E. & Dortch, J. Review of Devil's Lair artefact classification and radiocarbon chronology. *Aust. Archaeol.* **43,** 28–32 (1996).
22. Barnosky, A. D., Koch, P. L., Feranec, R. S., Wing, S. L. & Shabel, A. B. Assessing the causes of late Pleistocene extinctions on the continents. *Science* **306,** 70–75 (2004).
23. Field, J. H., Wroe, S., Trueman, C. N., Garvey, J. & Wyatt-Spratt, S. Looking for the archaeological signature in Australian megafaunal extinctions. *Quat. Int.* **285,** 76–88 (2013).
24. Wroe, S. *et al.* Climate change frames debate over the extinction of megafauna in Sahul (Pleistocene Australia–New Guinea). *Proc. Natl Acad. Sci. USA* **110,** 8777–8781 (2013).
25. Miller, G. H. *et al.* Pleistocene extinction of *Genyornis newtoni*: human impact on australian megafauna. *Science* **283,** 205–208 (1999).
26. Brook, B. W. *et al.* Lack of chronological support for stepwise prehuman extinctions of Australian megafauna. *Proc. Natl Acad. Sci. USA* **110,** E3368 (2013).
27. Cohen, T. *et al.* Hydrological transformation coincided with megafaunal extinction in central Australia. *Geology* **43,** 195–198 (2015).
28. Grün, R. *et al.* ESR and U-series analyses of faunal material from Cuddie Springs, NSW, Australia: implications for the timing of the extinction of the Australian megafauna. *Quat. Sci. Rev.* **29,** 596–610 (2010).
29. Balme, J., Davidson, I., McDonald, J., Stern, N. & Veth, P. Symbolic behaviour and the peopling of the southern arc route to Australia. *Quat. Int.* **202,** 59–68 (2009).

Supplementary Information is available in the online version of the paper.

Acknowledgements The fieldwork was undertaken with the approval of Adnyamathanha Traditional Lands Association (ATLA) and the South Australian Department of Aboriginal Affairs and Reconciliation. We thank for their contributions: A. Coulthard who participated in the fieldwork; R. Frank for his support both in the field and with drawing site maps; field assistants L. Foley and S. Adams; R. Cosgrove provided faunal advice; G. Robertson assisted with residue laboratory work; C. Brown assisted with graphic design, N. Bonney provided botanical advice; M. Raven and J. Webb carried out analyses of ochres; G. Medlin provided faunal advice; B. Barker provided botanical advice; P. Toms provided access to single grain OSL dating assessment; F. Williams for assistance in fieldwork and sample collection for optical dating; A. Couzens, W. Handley and G. Gully for their assistance with micro-CT imaging and photography of megafaunal specimens; and P. Veth, P. Hiscock, B. Cundy, W. Shawcross, S. Webb, J. Magee and D. Witter for critical feedback on the manuscript. This research was supported by Alinta Energy who provided financial support for fieldwork carried out in May 2013. L.A. and G.P. were supported by Australian Research Council Future Fellowship Grants FT130100195 and FT130101728, respectively. V.L. and Centre for Accelerator Science at ANSTO, acknowledge the support of the Australian Government through the National Collaborative Research Infrastructure Strategy (NCRIS). FWS is who - they did the drawing of the lithics and ought to be here.

Author Contributions G.H. conceived the project, supervised fieldwork, undertook data collection and analysis. L.A. provided chronological assessment for sediments and undertook the Bayesian age modelling. G.P. and T.W. identified megafaunal remains. D.Q. prepared chronological samples. N.S. advised on the results of chronological assessments. V.L. assisted with radiocarbon dating issues. E.F. provided fieldwork support and assisted in the analysis of stone artefact material. B.S. analysed and reported on stone artefact residues. V.C. and C.C. provided cultural advice and logistical support. C.C., S.W. and D.J assisted with fieldwork. G.H., P.M., L.A., G.P. and T.W. wrote the paper.

Author Information Reprints and permissions information is available at www.nature.com/reprints. The authors declare no competing financial interests. Readers are welcome to comment on the online version of the paper. Correspondence and requests for materials should be addressed to G.H. (A.R.A.S@bigpond.com).

METHODS

Excavation methods. Hand excavation was undertaken within Warratyi rock shelter (Extended Data Fig. 1a–c), using two 2 × 1 m trenches (Extended Data Fig. 1b, c). The first exploratory trench (squares 4C and 4D) was located on the southern side of the shelter to provide a cross-section through potential living areas from east to west (taking in part of the back wall). The second trench (squares 2B and 2C) was positioned in the centre of the shelter floor. Square 2B was only excavated down to spit 6 (30 cm) until obstructed by a large roof fall block.

Excavation was carried out using a 1-m grid system. This grid was further subdivided into 25 cm square units (quadrats: A–D Extended Data Fig. 1c) to enable greater recording precision. Excavation was undertaken using 5 cm spits, with a trowel and hand shovel and the excavated material was dry-sieved through (8, 5 and 2 mm) sieves. Stratigraphic features, such as charcoal lenses, ash or hearth-like lenses, were all drawn, photographed and noted during the excavation process. Detailed profile drawings were made on completion of the excavation. If possible, stone artefacts, bone and ochre were individually recorded and excavated from their *in situ* location and bagged separately, rather than being retrieved from the bulk sediment collected from individual spits. To reduce the potential for contamination of the excavated surfaces by loose material falling into the pit, the area surrounding each square (where possible) was covered with plastic sheeting and any loose spoil removed. Excavators were encouraged to wear soft shoes to reduce potential damage to the pit walls.

Each spit was recorded using a standard excavation sheet, which included making notes of the individual features and conditions encountered within each square and quadrat. A geomorphologist (P.M.) was present during the excavation process to advise excavators on the variability of sedimentary units and the positions of potential depositional changes associated with strata boundaries. When these depositional changes were detected during the excavation, they were noted and new strata were excavated as separate entities within a spit. This process reduced the potential for the sediment of two different strata being mixed.

Where a filled burrow (mostly attributable to rabbits) was encountered, the infilling sediment was removed as a discrete unit and bagged separately. These burrows were excavated in each square before the undisturbed enclosing sediments were excavated, thereby minimising potential contamination of the primary sediment by younger and/or mixed burrow infill material.

All *in situ* finds larger than 2 cm (including bone) were plotted in plan view within each excavated quadrat (A–D) and their depth ascertained by levelling within each spit (Extended Data Fig. 1b, c). Some of these *in situ* finds were photographed, however, most were not as their importance at the time of the excavation was not known (for example, bone point and *Diprotodon* bone fragments). All sediment removed from each spit was weighed. All material remaining on the sieves was bagged for further analysis. Bulk soil samples were removed for sedimentary analyses. At a later stage, sediment residues were wet-sieved through a 1-mm mesh before sorting. All charcoal, artefacts, bone fragments and plant matter recovered from this process were bagged. The location of charcoal samples collected during the excavation was plotted on plans, their depth recorded and then bagged separately.

A total of 1,070 stone artefacts were tested for refitting from square 2C in order to confirm the integrity of the apparently intact depositional laminae. These artefacts were assessed to see if they could be refitted together as parts of a former piece of stone artefact, on the assumption that their original separation was attributable to stone reduction activity and that they must have originated on a single surface in the shelter. All artefacts from square 2C that were greater than 10 mm in maximum dimension were assessed for refitting. Each refit set comprised artefacts that could be treated analytically as a single knapping episode[30]. As such, the distance between artefact elevations for each refitting set provides a proxy measure for the vertical displacement of cultural material through the deposit by human trampling and other post-depositional activty[31]. Refitting was attempted within a 1 × 1 m area, which represents only a sample of the occupied area and therefore is unlikely to capture an entire knapping event. In addition, artefacts will have undoubtedly been laterally dispersed as a result of repeated human and animal occupation; therefore we can predict that the overall percentage of refits (the 'success rate') will be low[32].

Optical dating of quartz grains. Seven optical dating samples were collected from cleaned exposures of excavation square 2C using metal tubes, and wrapped in light-proof bags for transportation and storage. Bulk sediment samples were also collected from the surrounding few centimetres of each sample tube for β-dose rate determination and water content analysis. In the laboratory, quartz grains of 180–212 μm diameter were extracted from the un-illuminated centres of the metal tubes under safe light (dim red LED) conditions and prepared for burial dose estimation using standard procedures[33], including etching by 48% hydrofluoric acid for 40 min to remove the α-irradiated external layers.

Two semi-independent approaches were used to obtain optical age estimates for the Warratyi samples. Single-grain optically stimulated luminescence (OSL) dating of quartz[34,35] was routinely applied to all samples, and was preferred over standard multiple-grain OSL dating because of its ability to identify insufficiently bleached grain populations[36,37], contaminant grains associated with post-depositional mixing[38], and aberrant grains displaying inherently unsuitable luminescence properties[39,40]. Single-grain TT-OSL dating of quartz[41–43] was applied to the oldest sample in the sequence (ERS-7) as a means of cross-checking the reliability of the OSL-dating approach over dose ranges of 150–200 Gy. TT-OSL dating was applied to individual grains of quartz rather than multi-grain aliquots in this study, following the reliable application of this approach at other archaeological cave and rock shelter sites[38,44,45].

OSL and TT-OSL equivalent dose (D_e) measurements were made using experimental apparatus and quality assurance criteria described previously[38,44]. Samples were irradiated with a Risø TL-DA-20 $^{90}Sr/^{90}Y$ β source that had been calibrated to administer known doses to multi-grain aliquots and single-grain discs. For single-grain measurements, spatial variations in the β-dose rate across the disc plane were taken into account by undertaking hole-specific calibrations using γ-irradiated quartz. Quartz grains with a diameter of 180–212 μm were measured in standard single-grain aluminium discs drilled with an array of 300 × 300 μm holes.

D_e values were determined for individual grains of quartz using the single-aliquot regenerative-dose (SAR) procedures[34] shown in Supplementary Table 3. Between 900 and 1,300 individual quartz grains of each sample were measured for D_e determination (Supplementary Table 4). Sensitivity-corrected dose–response curves were constructed using the first 0.17 s of each green-laser stimulation after subtracting a mean background count obtained from the last 0.25 s of the signal. A preheat of 260 °C for 10 s was used in the OSL SAR procedure before measuring the natural (L_n) and regenerative dose (L_x) signals, and a cut-heat of 160 °C was applied before undertaking the test-dose OSL measurements (T_n and T_x) (Supplementary Table 3). These preheating conditions yielded an accurate measured-to-recovered dose ratio of 1.03 ± 0.03 and a relatively low overdispersion value of 12 ± 3% for a ∼130 Gy dose-recovery test performed on individual grains of sample ERS-5 (Extended Data Fig. 6A). The single-grain TT-OSL SAR procedure (Supplementary Table 3) uses a TT-OSL test dose measurement rather than an OSL test-dose measurement (step 11) to correct for sensitivity change, following suitability assessments performed elsewhere[40,44–46]. A dose-recovery test performed on 1,200 individual quartz grains of sample ERS-7 attests to the general suitability of this SAR procedure (Extended Data Fig 6A). The TT-OSL dose-recovery test was performed on a batch of unbleached grains owing to the relatively long periods of light exposure needed to bleach natural TT-OSL signals down to low residual levels[47]. A known (172 Gy) laboratory dose of similar magnitude to the expected D_e was added on top of the natural signals for these grains. The recovered dose was then calculated by subtracting the weighted mean natural D_e of sample ERS-7 (168 ± 12 Gy; determined on a separate batch of grains and summarized in Supplementary Table 5) from the weighted mean D_e of these unbleached and dosed grains (350 ± 18 Gy). This approach yielded a net (that is, natural-subtracted) recovered-to-given ratio of 1.06 ± 0.09 for sample ESR-7. An overdispersion value of 12 ± 9% was calculated for the D_e distribution of the unbleached and dosed batch of grains, which is consistent with that obtained for the single-grain OSL dose-recovery test.

Individual D_e estimates are presented with their 1 standard error ranges (Supplementary Table 5 and Extended Data Fig. 6C), which have been derived from three sources of uncertainty: (i) a random uncertainty term arising from photon-counting statistics for each OSL or TT-OSL measurement, calculated using equation 3 from ref. 48; (ii) an empirically determined instrument-reproducibility uncertainty of 2% for each single-grain measurement; and (iii) a dose–response curve fitting uncertainty determined using 1,000 iterations of the Monte Carlo method implemented in Analyst[49].

Environmental dose rates have been calculated using a combination of *in situ* field γ-ray spectrometry and high-resolution γ spectrometry of dried and homogenized bulk sediments collected directly from the OSL-sampling positions. Cosmic-ray dose-rate contributions were calculated using the equations in ref. 50 after taking into consideration site altitude, geomagnetic latitude, density, thickness and geometry of the sediment or bedrock overburden. A small, assumed internal (α plus β) dose rate of 0.03 ± 0.01 Gy per kyr has been included in the final dose-rate calculations, based on published ^{238}U and ^{232}Th measurements for etched quartz grains from a range of locations[51–54] and an α efficiency factor (*a* value) of 0.04 ± 0.01 (refs 55–57). Radionuclide concentrations and specific activities have been converted to dose rates using published conversion factors[58], allowing for β-dose attenuation[59,60] where applicable.

Radiocarbon (^{14}C) dating of hearth charcoal and eggshell samples. Seventeen eggshell fragments (15 Dromaius, 2 megapode) and two large charcoal fragments associated with hearth features were used to derive the final ^{14}C chronology of SU1A to SU4. A range of other organic materials were initially submitted for ^{14}C analysis but these were considered unreliable based on stratigraphic or

methodological grounds, as detailed in Supplementary Information (radiocarbon dating). Samples were pretreated using acid–base–acid procedures and their ^{14}C contents were measured using accelerator mass spectrometry at the Waikato Radiocarbon Laboratory and the ANSTO Radiocarbon Facility. Uncalibrated eggshell and charcoal ^{14}C ages (Supplementary Table 7) are expressed in ^{14}C years before present (^{14}C yr BP, where BP is defined as 1950 AD) following standard reporting conventions[61]. Isotopic fractionation has been corrected for by using the measured $\delta^{13}C$ value of each sample. The ^{14}C age estimates have been calibrated with the internationally ratified southern hemisphere SHCal13 curve[62], using OxCal v4.2.4 (ref. 63). The calibrated ^{14}C age ranges (cal yr BP) are described as 95.4% probability ranges throughout.

Bayesian age modelling. Bayesian age modelling was used to integrate all stratigraphically reliable chronological information within a unified statistical framework and to derive combined age estimates for individual stratigraphic units. The Bayesian age model for Warratyi was constructed using OxCal v4.2.4 (ref. 63). A sequence-deposition model with nested phases of uniform prior duration and associated boundaries was used to derive a combined chronostratigraphic framework for the site, following the approach outlined previously[64]. The main depositional sequence incorporates the five stratigraphic units found at Warratyi (SU1A–SU4) in an ordered succession according to depth. Units have been represented as nested sequences within the broader depositional column as their overall stratigraphic ordering is sufficiently well preserved. Separate phases have been used to represent groupings of numerical ages within individual units. This approach was deemed necessary for SU2–SU4 because the ^{14}C and optical dating samples were collected from multiple excavation squares that exhibited potentially irregular or spatially heterogeneous stratigraphic relationships. The exact relative ordering of dating samples from each unit could therefore not be directly constrained in a vertical profile. SU1A and SU1B are internally heterogeneous and exhibit signs of inter-horizon mixing, as borne out by the multiple dose components of optical dating samples ERS-1, ERS-2 and ERS-3 (see Supplementary Information: chronology). This has prevented us from making any assumptions about relative chronological ordering of dated horizons within these units, although the relative ordering of SU1A and SU1B remains sufficiently clear. Groupings within SU1A and SU1B were therefore also nested as separate phases rather than sub-sequences.

Each stratigraphic unit has been represented by a single phase, with the exception of SU3. This unit is significantly thicker than the others at Warratyi and can be differentiated into two broad archaeo–palaeontological phases according to distinct changes in artefact content and bone abundance at a depth of approximately 60–65 cm (Fig. 2). Two separate phases were nested within the SU3 sequence to account for archaeological sub-structuring of the dated horizons. Boundaries were used to delineate the beginning and end of each stratigraphic unit. We have not, however, incorporated any prior depositional gaps in the sequence model as there is no direct evidence of unconformities at Warratyi. The entire site sequence has been constrained with a minimum age of 0 years before 1950 AD and a maximum age of 60 kyr before 1950 AD. The latter represents a conservative upper age estimate for this archaeological sequence and has been chosen to predate sufficiently the earliest existing evidence of human presence in Australia around $\leq$50 ka, as determined from an assessment of 26 early occupation sites across Sahul[65]. We note, however, that the Bayesian age model is largely insensitive to our choice of maximum age constraint given the range of likelihoods obtained on the lowest stratigraphic unit.

The ^{14}C data were input into the model as conventional ages (using the OxCal R_Date function) and were subsequently calibrated using the SHCal13 curve[62] as part of the modelling procedure. Modelled posterior ^{14}C age ranges are therefore presented in calendar years before 1950 AD (cal yr BP). To avoid introducing systematic errors in the posterior results, optical dating ages (calculated as kyr before sample collection in 2012 AD) were similarly converted to years before 1950 AD before their incorporation in the model.

The final Bayesian age model for Warratyi was run using the general outlier function[66], which is based on a Student's *t*-test distribution with 5 degrees of freedom. Prior outlier probabilities of 5% were equally assigned to all dating samples to identify potentially significant statistical outliers. Likelihood estimates that yielded posterior outlier probabilities >5% were not excluded from the final model but were proportionally down-weighted in the iterative Monte Carlo runs, thereby producing an averaged chronological model[66].

Use-wear and residue analyses. Use-wear studies were conducted using a hand-held polarizing Dino-Lite AM4815ZT microscope at magnifications of 30× to 230×. Additional high-power microscopic investigation using an Olympus BX51 at magnifications of 50× and 500× in brightfield and darkfield, were undertaken on seven artefacts. Within the overall study, six small samples of residue (approximately 10–20 μl) were extracted from margins or areas of interest on specific stone artefacts. Samples were extracted with pipettes using distilled water as the lifting medium and transferred to slides that had been pre-cleaned with ethanol. The Dino-lite was used to guide this process. Sample slides were dried under covers for 24 h and then stained with a 0.25% solution of picrosirius red using the protocols described previously[67]. A Leitz Dialux 22 microscope with polarizing capability was used to examine the stained slides. Residues were photographed in plane, part-polarized and cross-polarized light at a magnification of 400× using a Tucsen ISH 500 camera.

Data availability. All elements necessary to allow interpretation and replication of results, including full datasets and detailed experimental procedures are provided in the Supplementary Information. Fossils and archaeological material generated in this study will be deposited at the SA Museum and an Adnyamathanha Traditional Lands Association (ATLA)-keeping place within a 6–12-month time-frame and will be publicly accessible upon request with permission from ATLA and the corresponding author.

30. Larson, M. L. & Kornfeld, M. Chipped stone nodules: theory, method, and examples. *Lithic Technol.* **22,** 4–18 (1997).
31. Villa, P. Conjoinable pieces and site formation processes. *Am. Antiq.* **47,** 276–290 (1982).
32. Laughlin, J. P. & Kelly, R. L. Experimental analysis of the practical limits of lithic refitting. *J. Archaeol. Sci.* **37,** 427–433 (2010).
33. Aitken, M. J. *An Introduction to Optical Dating: the Dating of Quaternary Sediments by the Use of Photon-stimulated Luminescence* (Oxford Univ. Press 1998).
34. Murray, A. S. & Roberts, R. G. Determining the burial time of single grains of quartz using optically stimulated luminescence. *Earth Planet. Sci. Lett.* **152,** 163–180 (1997).
35. Bøtter-Jensen, L., Bulur, E., Duller, G. A. T. & Murray, A. S. Advances in luminescence instrument systems. *Radiat. Meas.* **32,** 523–528 (2000).
36. Olley, J. M., Pietsch, T. & Roberts, R. G. Optical dating of Holocene sediments from a variety of geomorphic settings using single grains of quartz. *Geomorphology* **60,** 337–358 (2004).
37. Arnold, L. J., Bailey, R. M. & Tucker, G. E. Statistical treatment of fluvial dose distributions from southern Colorado arroyo deposits. *Quat. Geochronol.* **2,** 162–167 (2007).
38. Arnold, L. J., Demuro, M. & Navazo Ruiz, M. Empirical insights into multi-grain averaging effects from 'pseudo' single-grain OSL measurements. *Radiat. Meas.* **47,** 652–658 (2012).
39. Demuro, M. *et al.* Optically stimulated luminescence dating of single and multiple grains of quartz from perennially frozen loess in western Yukon territory, Canada: comparison with radiocarbon chronologies for the late Pleistocene Dawson tephra. *Quat. Geochronol.* **3,** 346–364 (2008).
40. Demuro, M., Arnold, L. J., Froese, D. G. & Roberts, R. G. OSL dating of loess deposits bracketing Sheep Creek tephra beds, northwest Canada: dim and problematic single-grain OSL characteristics and their effect on multi-grain age estimates. *Quat. Geochronol.* **15,** 67–87 (2013).
41. Wang, X. L., Wintle, A. G. & Lu, Y. C. Thermally transferred luminescence in fine-grained quartz from Chinese loess: basic observations. *Radiat. Meas.* **41,** 649–658 (2006).
42. Arsuaga, J. L. *et al.* Neandertal roots: cranial and chronological evidence from Sima de los Huesos. *Science* **344,** 1358–1363 (2014).
43. Demuro, M., Arnold, L. J., Parés, J. M. & Sala, R. Extended-range luminescence chronologies suggest potentially complex bone accumulation histories at the Early-to-Middle Pleistocene palaeontological site of Huéscar-1 (Guadix-Baza basin, Spain). *Quat. Int.* **389,** 191–212 (2015).
44. Arnold, L. J. *et al.* Luminescence dating and palaeomagnetic age constraint on hominins from Sima de los Huesos, Atapuerca, Spain. *J. Hum. Evol.* **67,** 85–107 (2014).
45. Demuro, M. *et al.* New luminescence ages for the Galería Complex archaeological site: resolving chronological uncertainties on the acheulean record of the Sierra de Atapuerca, northern Spain. *PLoS One* **9,** e110169 (2014).
46. Stevens, T., Buylaert, J.-P. & Murray, A. S. Towards development of a broadly-applicable SAR TT-OSL dating protocol for quartz. *Radiat. Meas.* **44,** 639–645 (2009).
47. Tsukamoto, S., Duller, G. A. T. & Wintle, A. G. Characteristics of thermally transferred optically stimulated luminescence (TT-OSL) in quartz and its potential for dating sediments. *Radiat. Meas.* **43,** 1204–1218 (2008).
48. Galbraith, R. F. A note on the variance of a background-corrected OSL count. *Ancient TL* **20,** 49–51 (2002).
49. Duller, G. A. T. Assessing the error on equivalent dose estimates derived from single aliquot regenerative dose measurements. *Ancient TL* **25,** 15–24 (2007).
50. Prescott, J. R. & Hutton, J. T. Cosmic ray contributions to dose rates for luminescence and ESR dating: large depths and long-term time variations. *Radiat. Meas.* **23,** 497–500 (1994).
51. Mejdahl, V. Internal radioactivity in quartz and feldspar grains. *Ancient TL* **5,** 10–17 (1987).
52. Bowler, J. M. *et al.* New ages for human occupation and climatic change at Lake Mungo, Australia. *Nature* **421,** 837–840 (2003).
53. Jacobs, Z., Duller, G. A. T. & Wintle, A. G. Interpretation of single-grain D_e distributions and calculation of D_e. *Radiat. Meas.* **41,** 264–277 (2006).
54. Pawley, S. M. *et al.* Age limits on Middle Pleistocene glacial sediments from OSL dating, north Norfolk, UK. *Quat. Sci. Rev.* **27,** 1363–1377 (2008).

55. Questiaux, D. Optical dating of loess: comparisons between different grain size fractions for infrared and green excited wavelengths. *Nucl. Tracks Radiat. Meas.* **18,** 133–139 (1991).
56. Rees-Jones, J. Optical dating of young sediments using fine-grain quartz. *Ancient TL* **13,** 9–14 (1995).
57. Rees-Jones, J. & Tite, M. S. Optical dating results for British archaeological sediments. *Archaeometry* **39,** 177–187 (1997).
58. Guérin, G., Mercier,N. & Adamiec, G. Dose-rate conversion factors: update. *Ancient TL* **29,** 5–8 (2011).
59. Mejdahl, V. Thermoluminescence dating: beta-dose attenuation in quartz grains. *Archaeometry* **21,** 61–72 (1979).
60. Brennan, B. J. Beta doses to spherical grains. *Radiat. Meas.* **37,** 299–303 (2003).
61. Stuiver, M. & Polach, H. A. Reporting of ^{14}C data. *Radiocarbon* **19,** 355–363 (1977).
62. Hogg, A. G. *et al.* SHCal13 Southern Hemisphere calibration 0–50,000 years cal bp. *Radiocarbon* **55,** 1889–1903 (2013).
63. Bronk Ramsey, C. Radiocarbon calibration and analysis of stratigraphy: the OxCal program. *Radiocarbon* **37,** 425–430 (1995).
64. Macken, A. C., Staff, R. A. & Reed, E. H. Bayesian age-depth modelling of Late Quaternary deposits from Wet and Blanche Caves, Naracoorte, South Australia: a framework for comparative faunal analyses. *Quat. Geochronol.* **17,** 26–43 (2013).
65. O'Connell, J. F. & Allen, J. The process, biotic impact, and global implications of the human colonization of Sahul about 47,000 years ago. *J. Archaeol. Sci.* **56,** 73–84 (2015).
66. Bronk Ramsey, C. Dealing with offsets and outliers in radiocarbon dating. *Radiocarbon* **51,** 1023–1045 (2009).
67. Stephenson, B. A modified Picro-Sirius Red (PSR) staining procedure with polarization microscopy for identifying collagen in archaeological residues. *J. Archaeol. Sci.* **61,** 235–243 (2015).

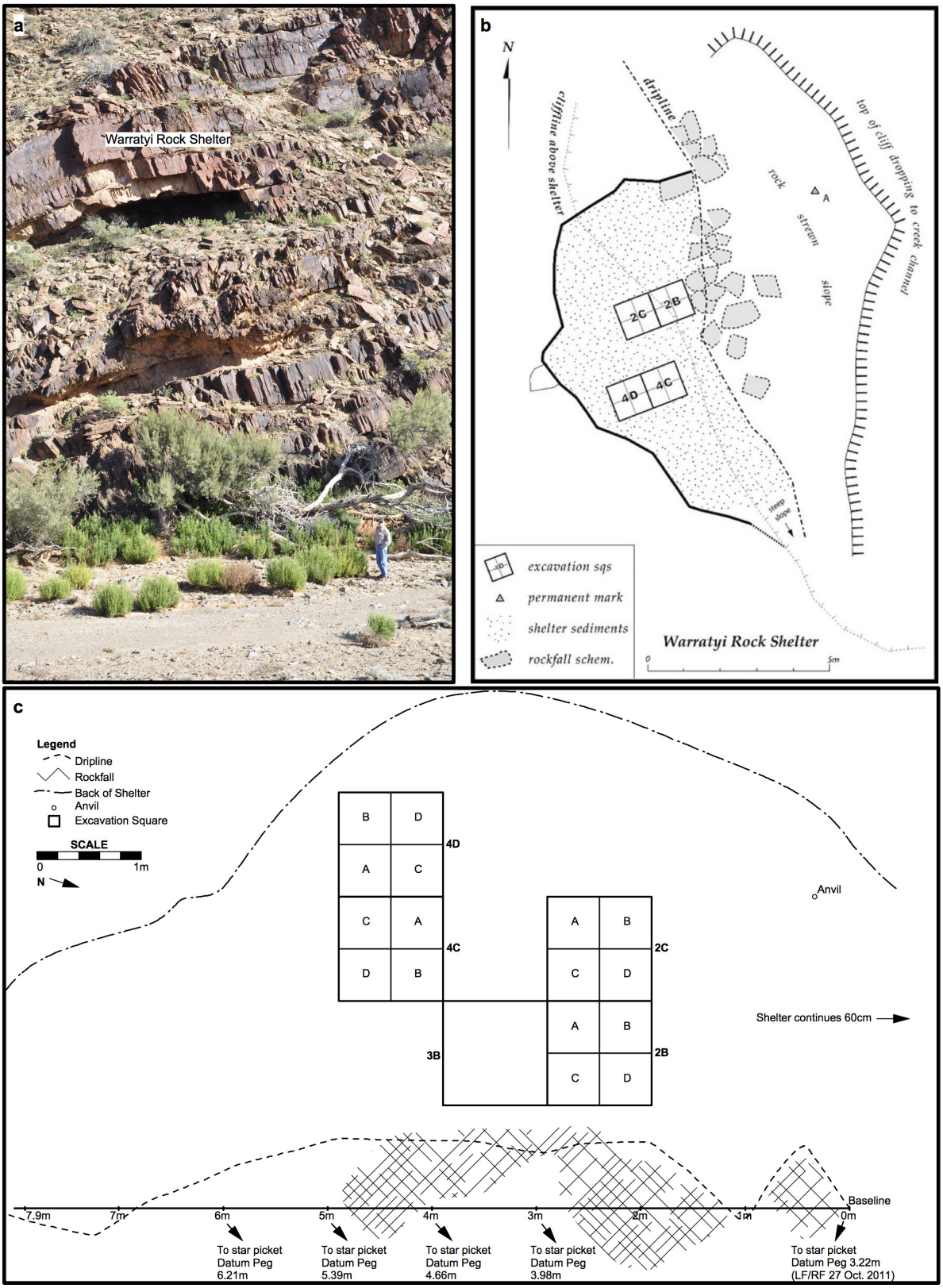

Extended Data Figure 1 | Warratyi rock shelter, site location, site plan and excavation strategy. a, Warratyi rock shelter above a dry creek bed, looking west at the main ridge profile and rocky bench at the front of the shelter. **b**, Plan of Warratyi rock shelter showing layout of excavation. Excavation squares (4D/4C and 2C/2B) have a surface area of 1 m^2. Drawing by R. Frank. **c,** Warratyi rock shelter excavation plan showing the layout of the excavation squares and 25 cm × 25 cm (A–D) quadrat units within each square.

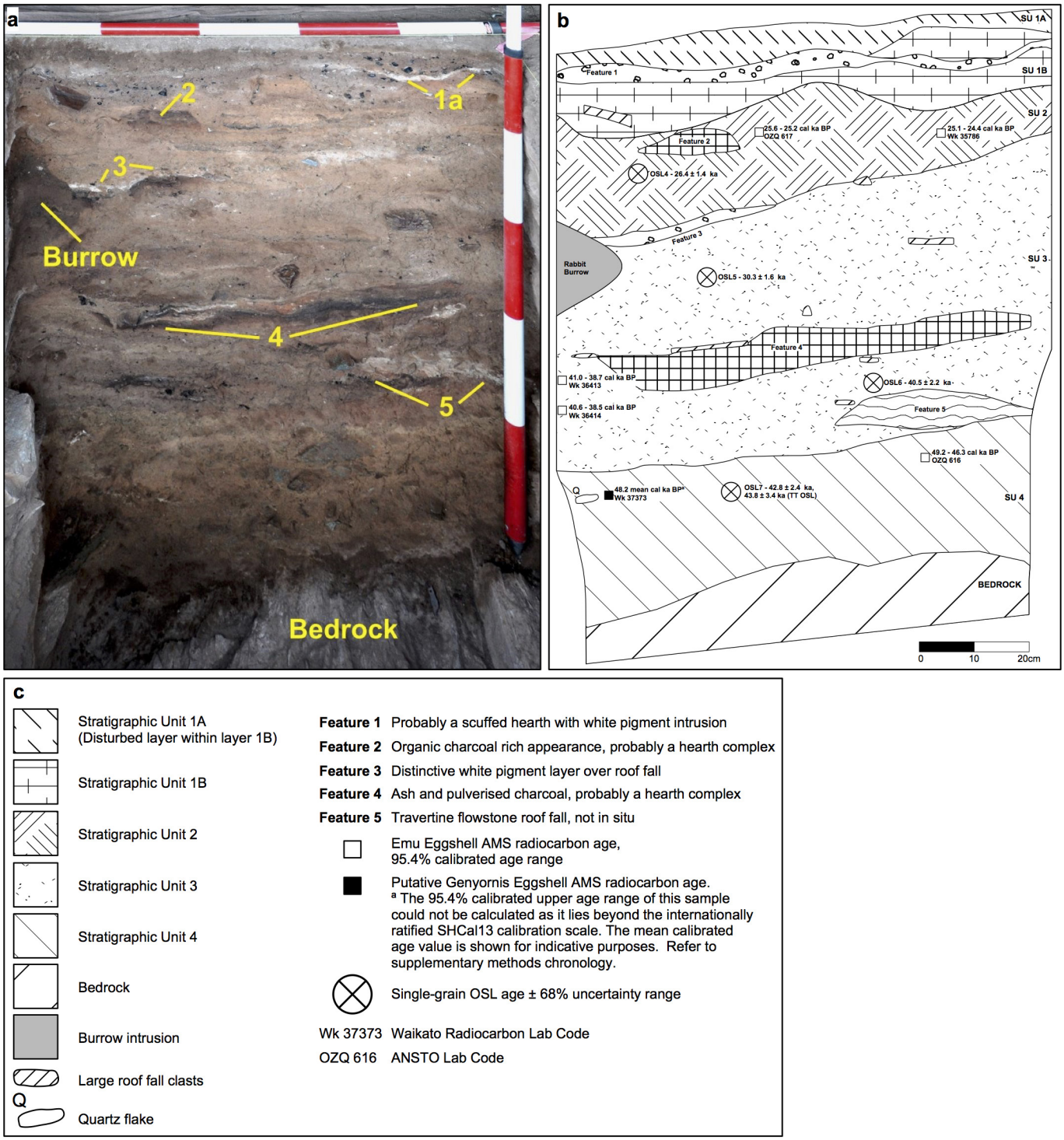

Extended Data Figure 2 | Excavation profiles and section drawings of Warratyi rock shelter square 2C. a, Profile of the west face of square 2C from the surface to the weathered bedrock on the floor of the shelter. Several charcoal concentrations and small lenticular features of ash and charcoal were interpreted as hearths. Roof fall flakes occur throughout and the only evidence of burrowing is the small, darker grey area on the left edge, which was traced across the excavation and identified as a rabbit burrow. This material was excavated separately to limit contamination of the main deposit. The numbers shown here denote the features shown in the profile drawing in **b**. The scale bar is marked with 20 cm units. **b**, Stratigraphic profile drawing of square 2C showing general stratigraphic features with feature descriptions and stratigraphic unit descriptions. **c**, Legend for stratigraphic profile drawing of square 2C. The scale bar is marked with 20 cm units.

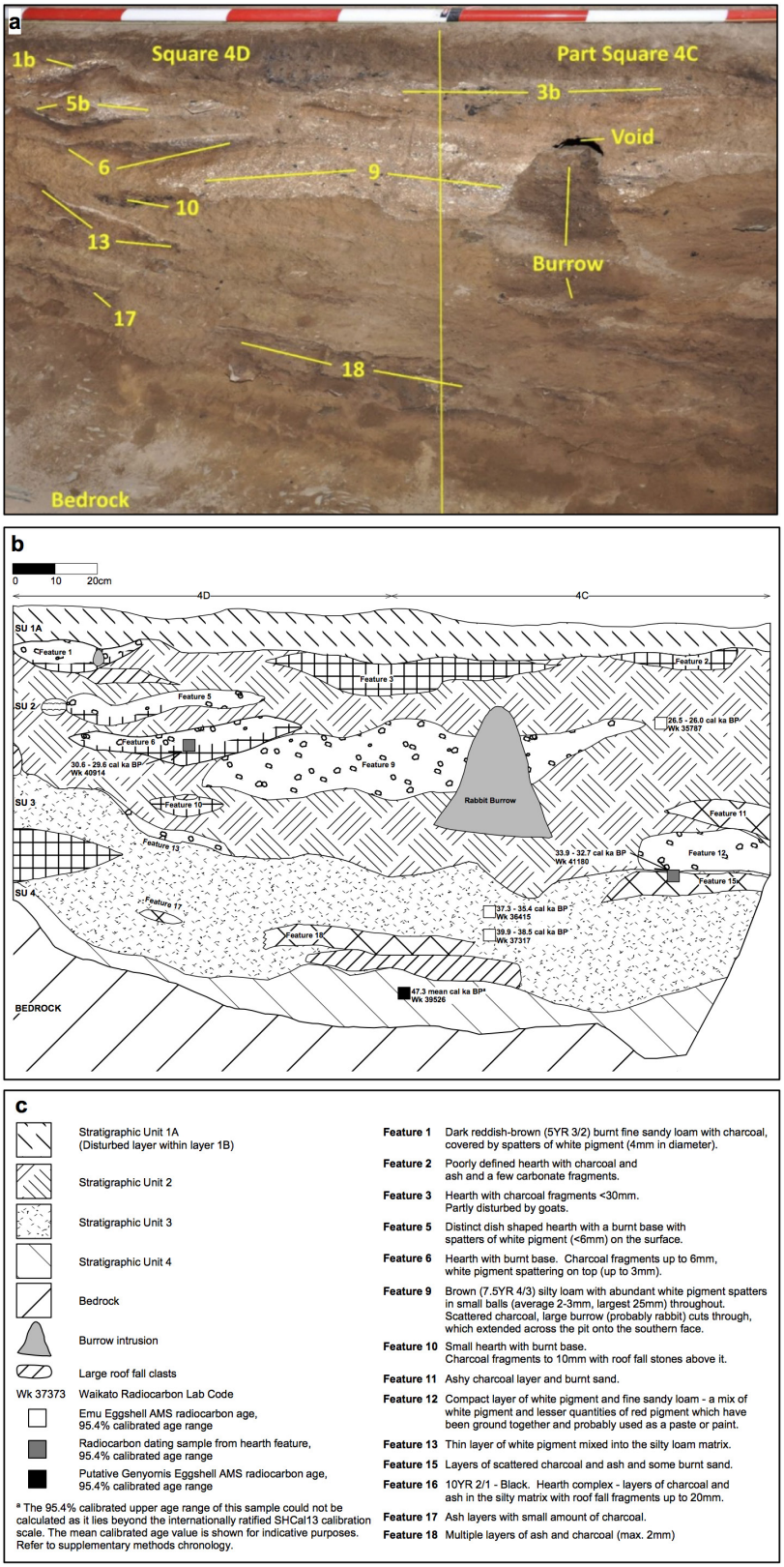

Extended Data Figure 3 | Excavation profiles and section drawings of Warratyi rock shelter squares 4C and 4D. a, Profile of the north face of square 4D and part of 4C (right of centre). All stratigraphic units are visible. A cross-section of the identified rabbit burrow is prominent in 4C; this disturbance, however, is limited and the burrow fill was excavated separately. Continuous concentrations of white pigment (9: gypsum spheres and pellets) are visible on either side of the burrow, attesting to the stratigraphic integrity of the surrounding deposits. The numbers shown here correspond to the features noted in **b** and **c**, drawing and legend respectively. The scale bar is marked with 20 cm units. **b**, Profile drawing of excavated squares 4C and 4D, depicting the stratigraphy visible in **a**. A rabbit burrow is located in the centre of the drawing in square 4C. Vertical and horizontal scales are equal. **c**, Legend for stratigraphic profile drawing of squares 4C and 4D.

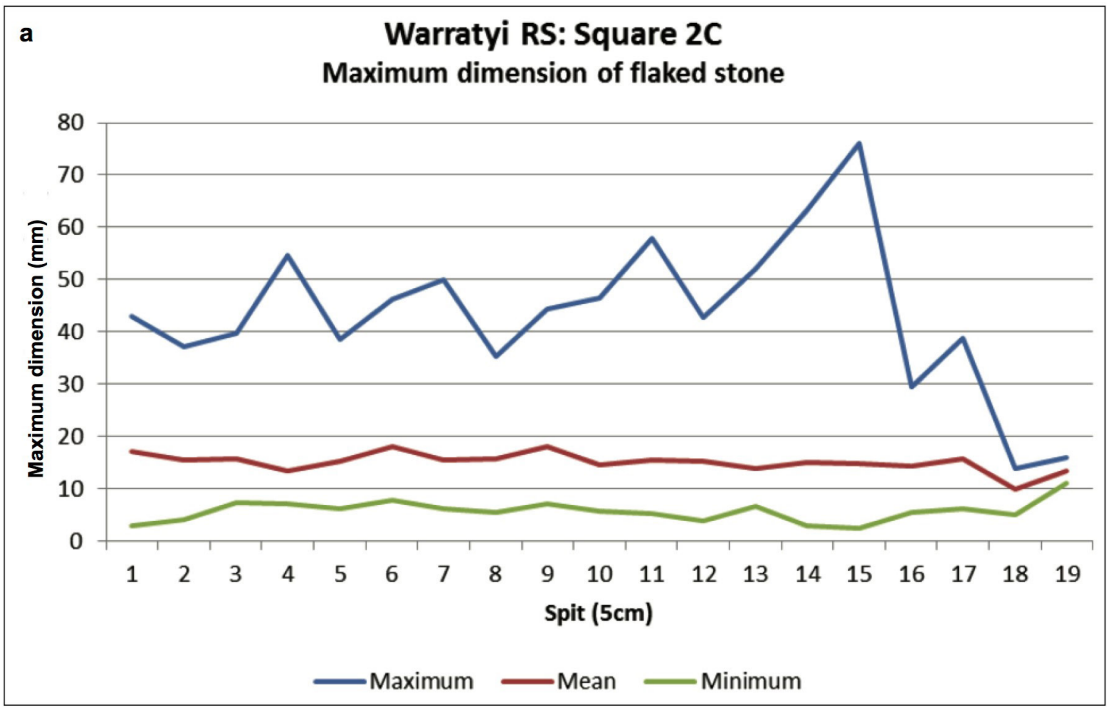

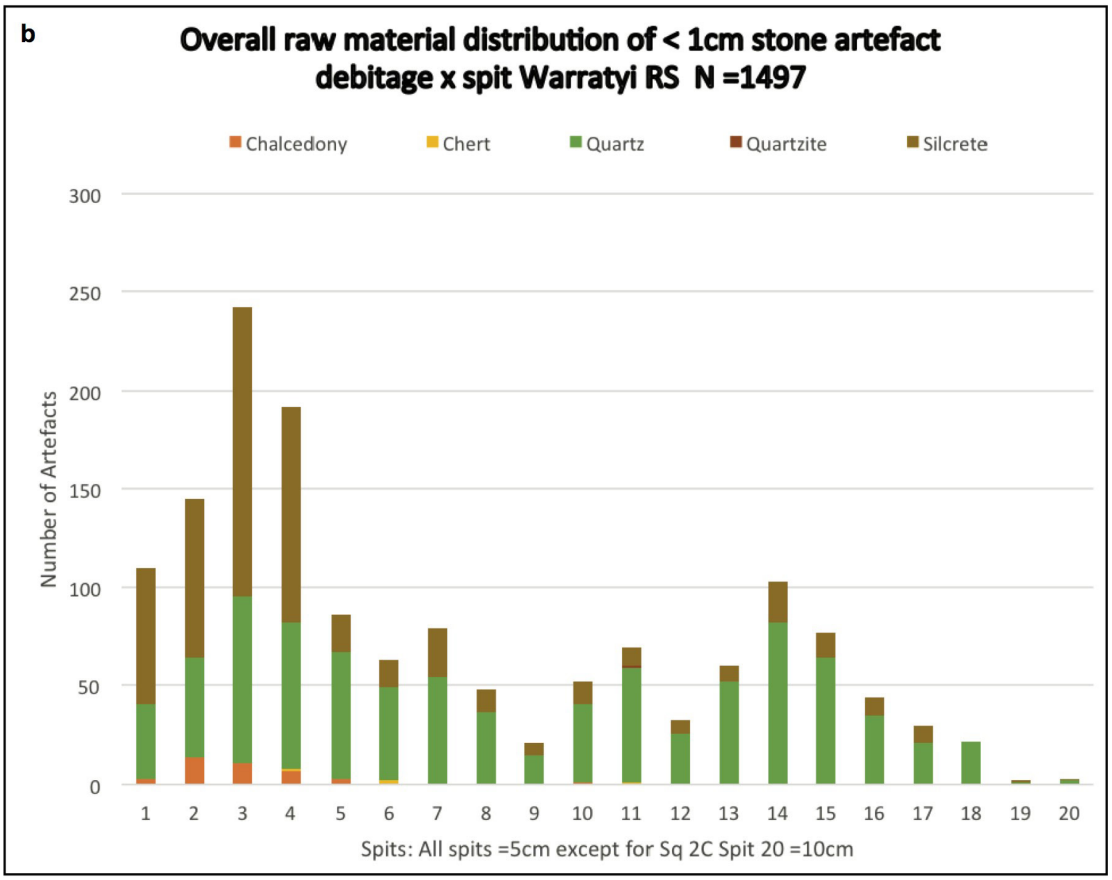

Extended Data Figure 4 | Graphical representation of the size of stone artefacts and distribution of raw materials in Warratyi rock shelter. **a**, Distribution of lengths for *in situ* >1 cm artefacts found at Warratyi rock shelter. Blue line, maximum length; grey line, mean; orange, minimum length. **b**, Distribution of raw material types for stone artefacts <1 cm in length by spit at Warratyi rock shelter. Orange, chalcedony; green, quartz; brown, silcrete; yellow, chert.

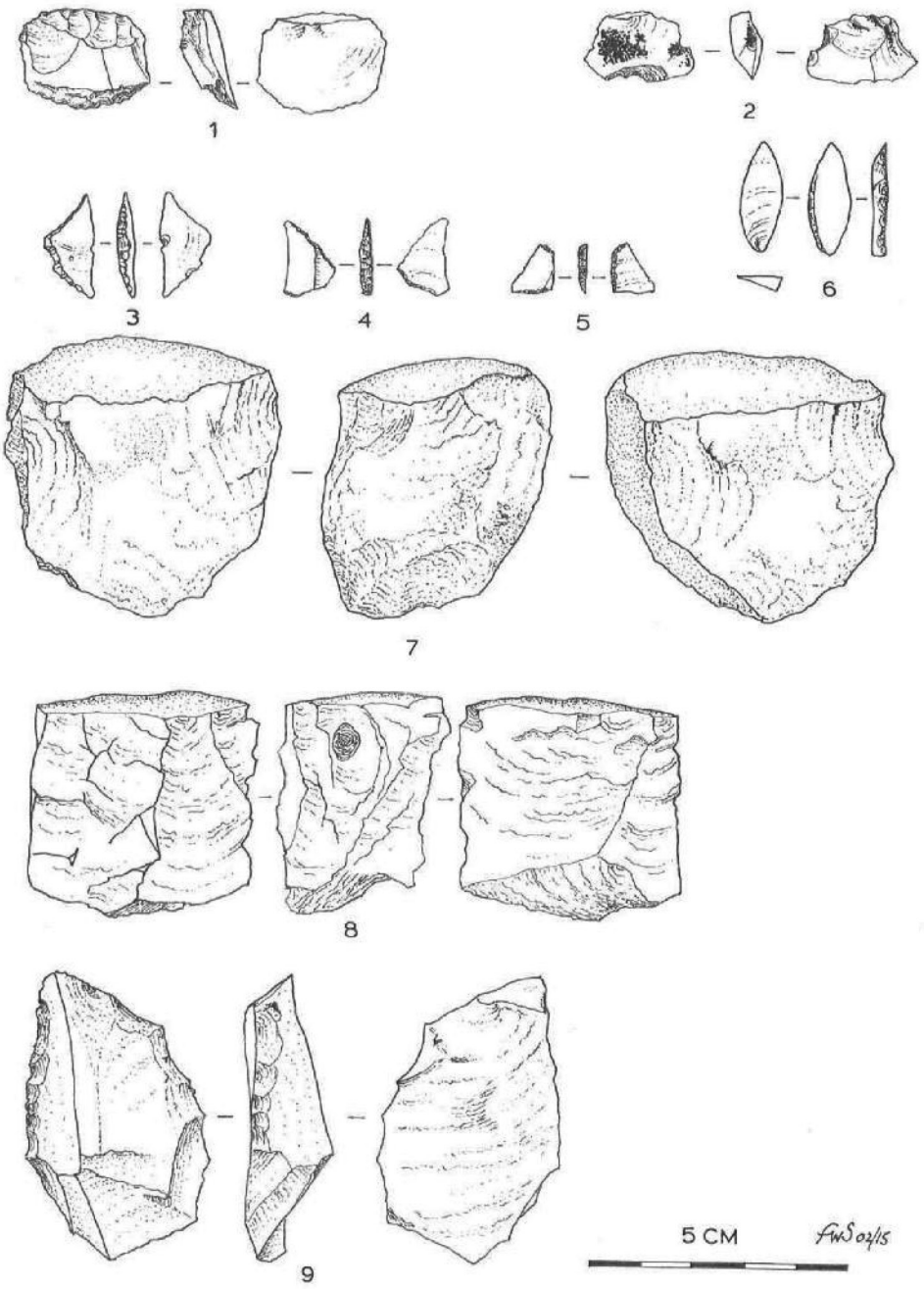

Extended Data Figure 5 | A sample of the stone artefacts found in Warratyi rock shelter. Drawing of select Warratyi stone artefacts.1, Adze flake, chalcedony, square 2C, spit 4. 2, Adze flake, chalcedony, square 2C, spit 5, retains patches of resinous adhesive. 3, Geometric, backed artefact, silcrete, square 2B, spit 5. 4, Geometric, backed artefact, silcrete, square 2B, spit 5. 5, Geometric, backed artefact, silcrete, square 2B, spit 5. 6, Flake with backing on one edge, silcrete, square 2B, spit 5. 7, Core, rolled quartz pebble, square 4C, spit 9. 8, Core, rolled quartz pebble, square 4C, spit 15. 9, Retouched, quartzite flake, square 2C, spit 15.

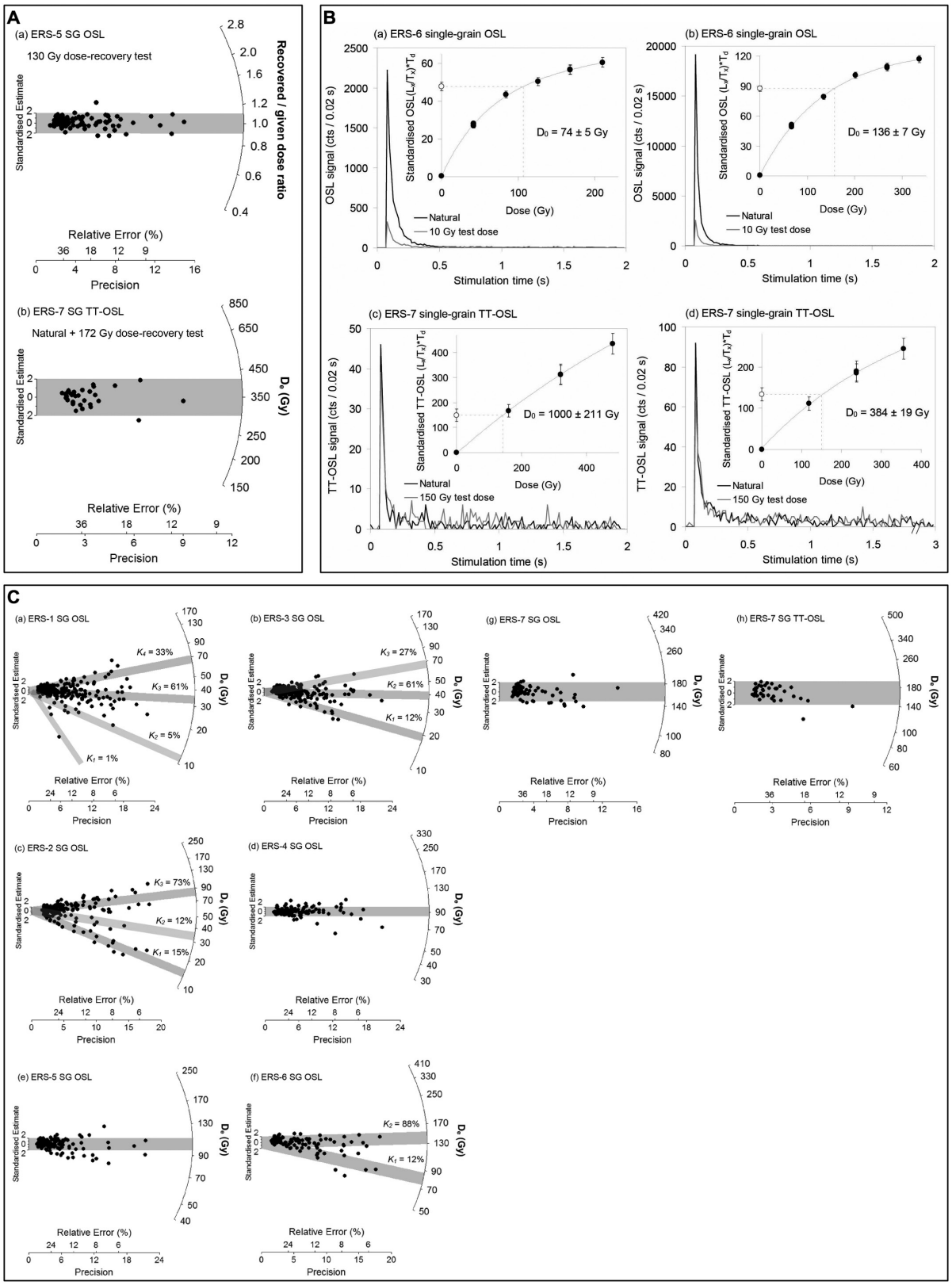

Extended Data Figure 6 | See next page for caption.

Extended Data Figure 6 | Single-grain OSL dose-recovery and single-grain OSL and TT-OSL D_e distribution results for Warratyi rock shelter A, Single-grain OSL and TT-OSL dose-recovery test results. **Aa**, Radial plot showing the recovered to given dose ratios obtained for individual quartz grains of ESR-5 using the OSL SAR procedure (Supplementary Table 3). The natural OSL signals of these grains were first optically bleached with two 1,000-s blue LED illuminations at ambient temperature, each separated by a 10,000 s pause. The grey shaded region on the radial plot is centred on the administered dose for each grain (sample average = 130 Gy). **Ab**, Radial plot showing the dose-recovery test (natural + dosed) D_e values obtained for individual quartz grains of ESR-7 using the TT-OSL SAR procedure (Supplementary Table 3). The single-grain natural signals were not bleached during the TT-OSL dose-recovery test. Instead, a known dose of similar magnitude to the expected D_e was added on top of the natural signals. **B**, Representative OSL or TT-OSL decay and dose–response curves for individual quartz grains from Warratyi rock shelter. **Ba**, Quartz grain from sample ERS-6 with an average OSL signal ($T_n \approx 800$ counts per 0.17 s). **Bb**, Quartz grain from sample ERS-6 with a relatively bright OSL signal ($T_n \approx 5{,}000$ counts per 0.17 s). **Bc**, Quartz grain from sample ERS-7 with an average TT-OSL signal ($T_n \approx 100$ counts per 0.17 s). **Bd**, Quartz grain from sample ERS-7 with a relatively bright TT-OSL signal ($T_n \approx 200$ counts per 0.17 s). In the insets, open circles denote the sensitivity-corrected natural OSL or TT-OSL signals, and filled circles denote the sensitivity-corrected regenerated OSL or TT-OSL signals. D_0 values characterize the rate of signal saturation with respect to administered dose and equate to the dose value for which the saturating exponential dose–response curve slope is $1/e$ (or ~0.37) of its initial value. **C**, Single-grain OSL and TT-OSL D_e distributions for the Warratyi rock shelter samples. Grey bands are centred on the D_e values derived using either the central age model (samples ERS-4 (**Cc**), ERS-5 (**Ce**), ERS-7(**Cg**)), or the finite-mixture model (samples ERS-1 (**Ca**), ERS-2 (**Cb**), ERS-3 (**Cc**), ERS-6(**Cf**)). Percentage of grains associated with each finite-mixture model component (k_n) are shown in **Ca**, **Cb**, **Cc** and **Cf**.

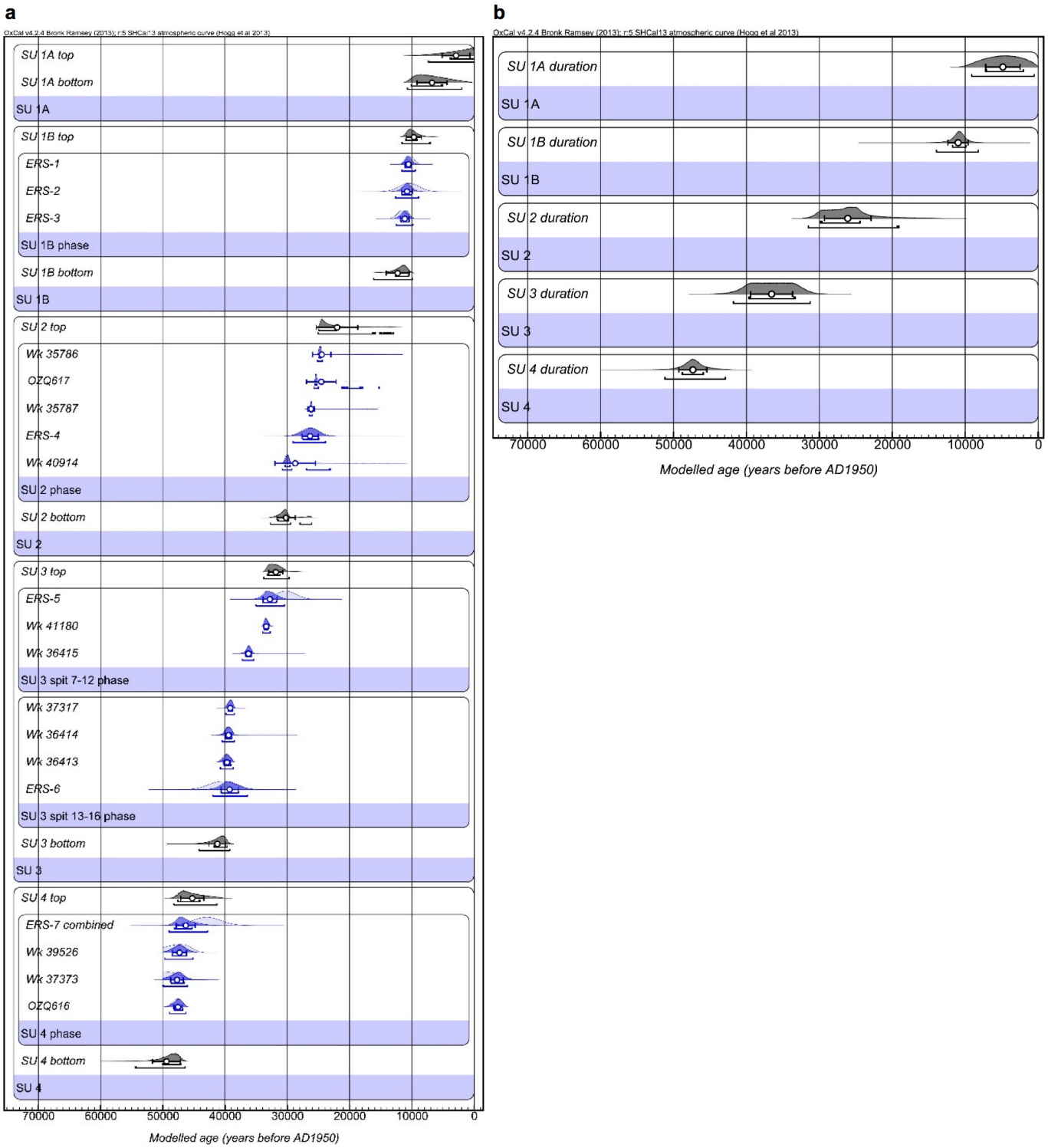

Extended Data Figure 7 | Bayesian modelling results for Warratyi rock shelter. a, Bayesian modelling of optical-dating and ^{14}C results from Warratyi rock shelter. The prior age distributions for the dating samples (likelihoods) are shown as light blue probability density functions (PDFs). The modelled posterior distributions for the dating sample and stratigraphic unit boundaries are shown as dark blue and grey PDFs, respectively. Optical dating and ^{14}C ages are shown on a calendar year timescale and both are expressed in years before 1950 AD. The ^{14}C data were input into the model as conventional ages and were subsequently calibrated using the SHCal13 curve[64] as part of the modelling procedure. The white circles and associated error bars represent the mean ages and 1 standard error uncertainty ranges of the PDFs. The 68.2% and 95.4% ranges of the highest posterior probabilities are indicated by the horizontal bars underneath the PDFs. **b**, Bayesian-modelled durations of the stratigraphic units at Warratyi rock shelter. The PDFs have been calculated from the modelled posterior probabilities of the upper and lower boundaries of each stratigraphic unit (shown as grey PDFs in plot **a** using the difference query function in OxCal v4.2.4.

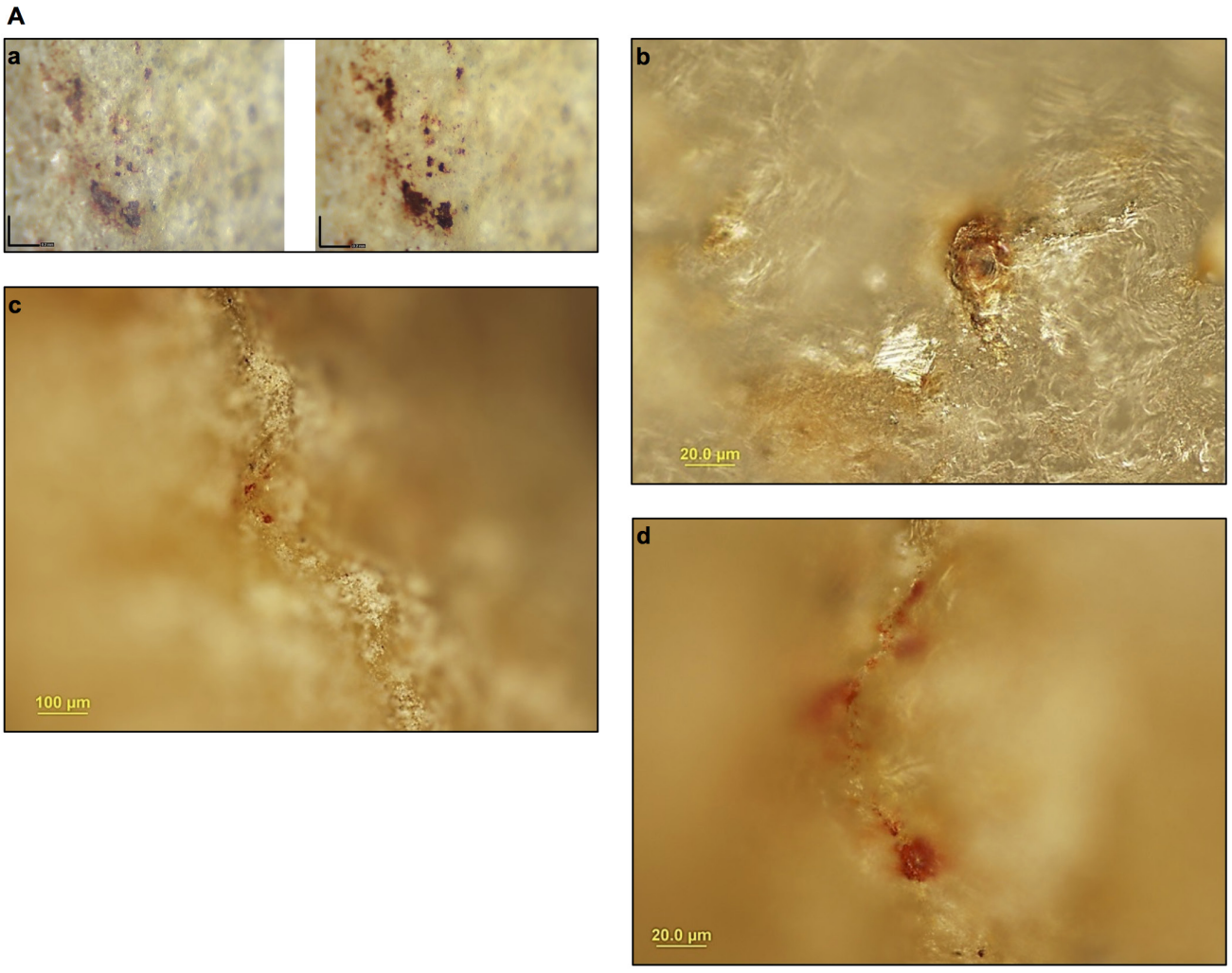

Extended Data Figure 8 | Distribution of resin and red ochre material on stone artefacts and gypsum analysis. Aa, Resin adhering to the medial arris ridge that runs the length of the dorsal surface at 215× magnification in plane (pp, left) and cross polarized (xp, right). Scale bar, 0.2 mm. **Ab**, Resin with carbonized inclusions and associated hafting polish 500× darkfield. Scale bar, 20 µm. **Ac**, Ocre grains within the worked margin; 50× darkfield. Scale bar, 100 µm. **Ad**, Worked ochre grains; 500× brightfield cross polarized. Scale bar, 20.0 µm. **Ba**, Spheres of gypsum lying *in situ* within excavated square 4C, Warratyi rock shelter. **Bb**, Scanning electron microscope image of gypsum from Warratyi rock shelter. The sample consisted of very fine-grained clear gypsum-cleavage plates, mostly sub-equidimensional to slightly tabular and 5–10 µm across. There are occasional larger tabular–acicular (needle-like) fragments up to 100 µm long. Scattered through the gypsum are well-rounded, sub-spherical silt-sized grains of quartz 50–75 µm across, generally reddish in colour. Scale bar, 1 µm.

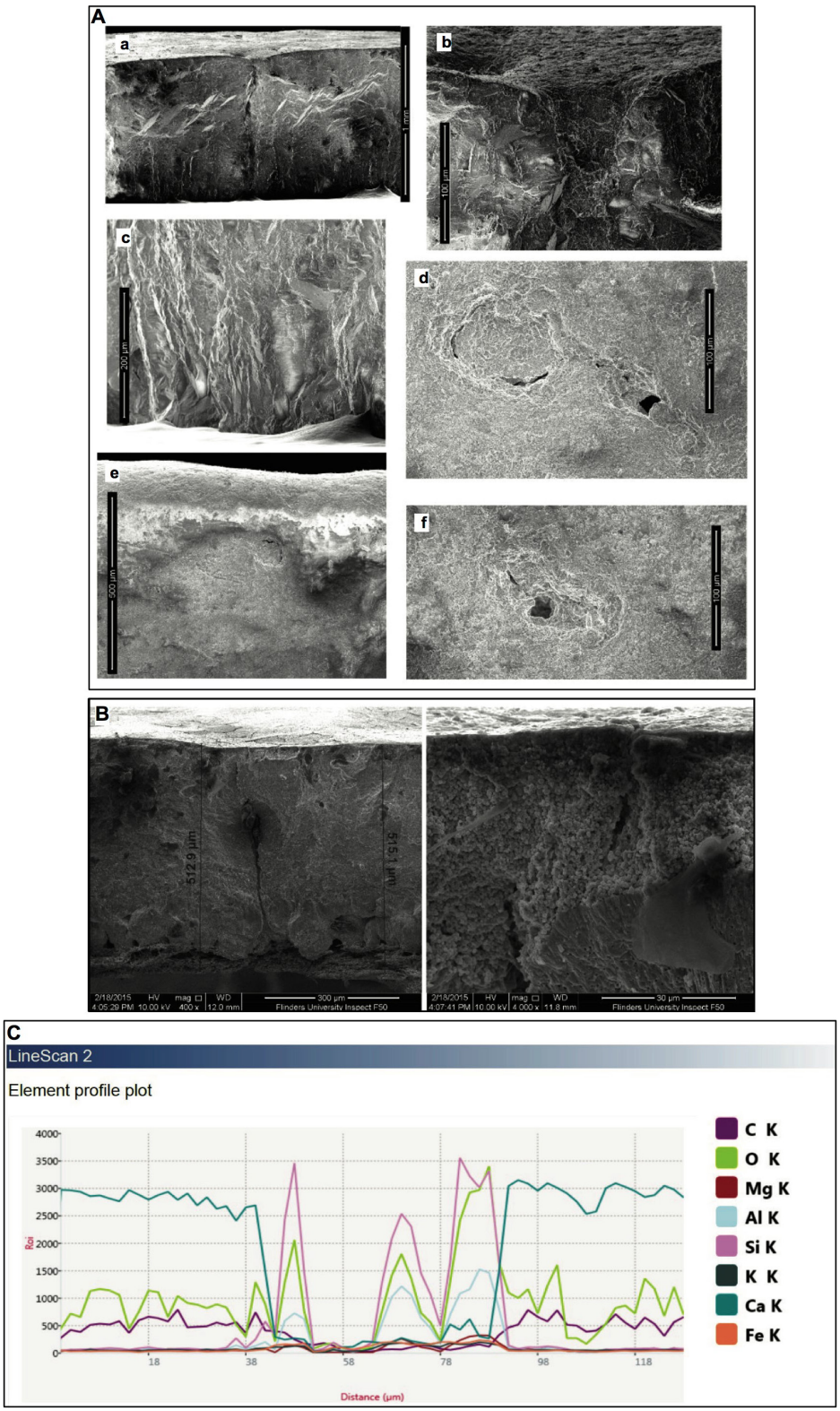

Extended Data Figure 9 | Analysis of putative *Genyornis* oological eggshell material. A, Scanning electron micrographs of sample 1 from square 4C, quadrat B, spit 18. **Aa**, view of a fresh broken edge showing a smooth eroded-out surface (upper), a section through a pore canal; **Ab**, detail of the pore canal opening showing the material filling pore; **Ac**, detail of the inner layer 1 and smooth inner surface of the shell showing that it is slightly eroded, so that the tips of the mammillary cones of layer 1 are lost; **Ad**, outer surface of the shell showing an elongated pair of pore canal openings occluded by material; **Ae**, outer surface of the shell showing the rounded eroded edge of the fragment; **Af**, outer surface of the shell and another opening to a pore canal showing its elongated nature and occlusion by material. **B**, Scanning electron micrograph views of an eggshell of *Anseranas semipalmata* (sample from the South Australia Museum B.14591) showing the cross-section on the left and a detail of the accessory layer on the right. Note that the accessory layer comprises an amorphous mass of similar sized spheres, a structure that typifies the accessory layer of many galloanseres, including that of putative *Genyornis* material. **C**, Element-profile plot across the pore aperture shown in **Ab**. The sides of the pore are at approximately 40 and 90 µm on the *x* axis and on either side the profile reflects the dominant $CaCO_3$ nature of eggshell. Within the pore, elevated levels of iron (Fe), silica (Si) and aluminium (Al) are present.

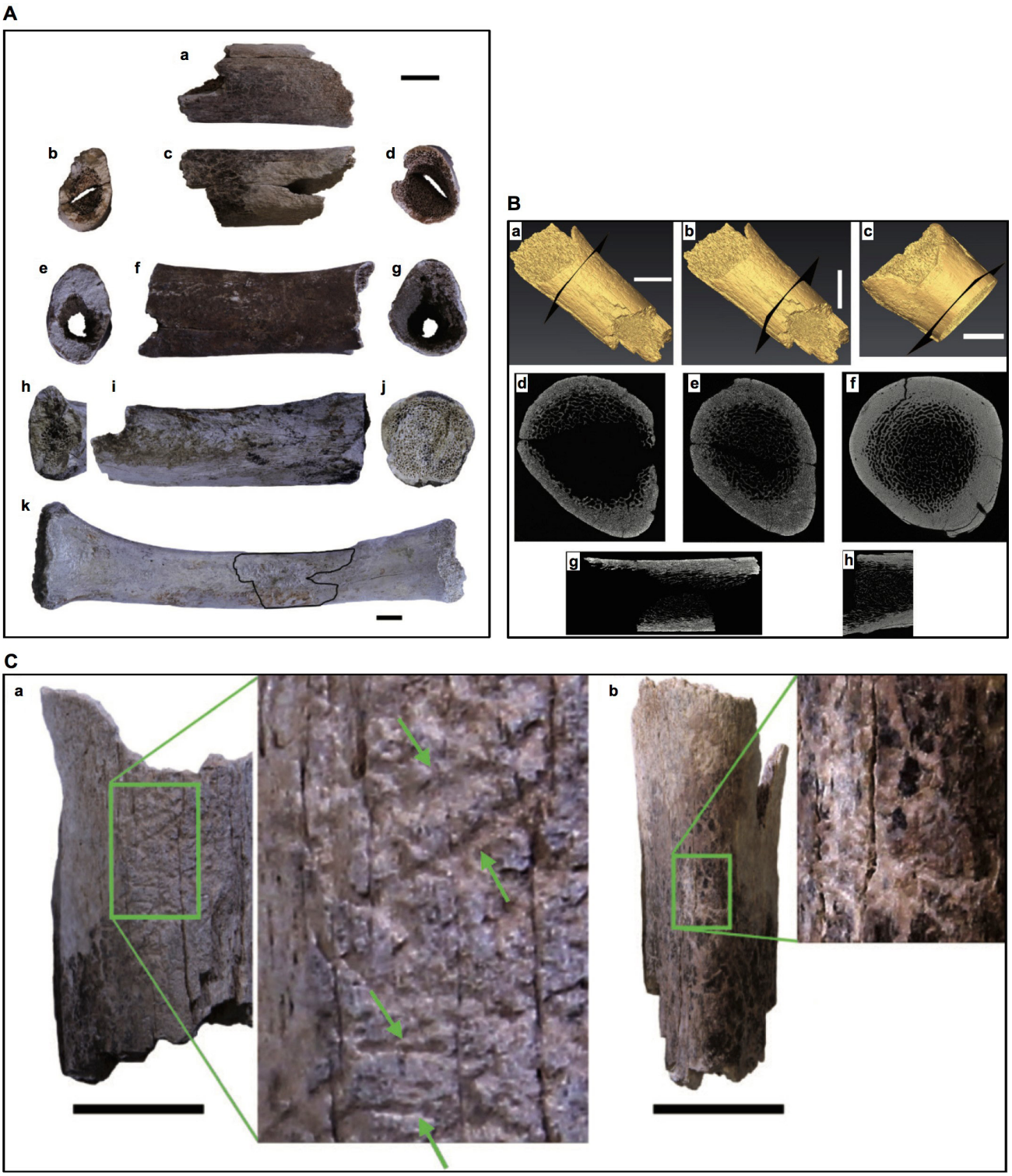

Extended Data Figure 10 | Megafaunal bone evidence of *D. optatum*. **A**, Comparison between the *Diprotodon* bone (EMU RS-6737-7754) from Warratyi rock shelter and juvenile radius specimens of *D. optatum* from the South Australian Museum (SAMA P51340–P51342). **Aa**, EMU RS-6737-7754 in anterior view. **Ab**, View of the broken distal end of EMU RS-6737-7754. **Ac**, EMU RS-6737-7754 in posterior view. **Ad**, View of the broken proximal end of EMU RS-6737-7754. **Ae**, View of the broken distal end of SAMA P51340. **Af**, SAMA P51340 in posterior view. **Ag**, View of the broken proximal end of SAMA P51341. **Ah**, View of the broken distal end of SAMA P51341. **Ai**, SAMA P51341 in posterior view. **Aj**, View of the broken proximal end of SAMA P51340. **Ak**, SAMA P51342 in posterior view. The silhouette represents the approximate corresponding position for EMU RS-6737-7754. Scale bars, 20 mm. The top scale bar is for panels **Aa**–**Aj**; the bottom scale bar is for panel **Ak**. **B**, Micro-computed tomographic images comparing EMU RS-6737-7754 with a juvenile radius specimen of *D. optatum*. **Ba**, Isosurface rendering of EMU RS-6737-7754 showing the position of a more proximal cross-section. **Bb**, Isosurface rendering of EMU RS-6737-7754 showing the position of a more distal cross-section. **Bc**, Isosurface rendering of SAMA P51341 showing the position of the cross-section. **Bd**, More proximal cross-section of EMU RS-6737-7754 (as shown in **Ba**). **Be**, More distal cross-section of EMU RS-6737-7754 (as shown in **Bb**). **Bf**, Cross-section of SAMA P51341 (as shown in **Bc**). **Bg**, Longitudinal-section of EMU RS-6737-7754. **Bh**, Longitudinal-section of a portion of SAMA P51341. Scale bars, 20 mm. C, Taphonomic markings on the surface of EMU RS-6737-7754.